

Quantifying the anisotropic density structure of the Central Molecular Zone – a 2D correlation function approach

Xiu-Yu Cai^{1,2}, Guang-Xing Li³ and Lei Qian^{1,2}

¹ University of Chinese Academy of Sciences, Beijing 100049, China

² National Astronomical Observatories, Chinese Academy of Sciences, Beijing 100101, China; Lei Qian:
lqian@nao.cas.cn

³ South-Western Institute for Astronomy Research, Yunnan University Kunming, 650500 Yunnan, P.R.
China; *gxli@ynu.edu.cn*

Received 20xx month day; accepted 20xx month day

Abstract The Central Molecular Zone (CMZ) is a ring-like structure sitting at the center of the Milky Way. Using the 870 μm continuum map from the APEX Telescope Large Area Survey of the Galaxy (ATLASGAL), we study the anisotropy of the density structure of the gas in the Central Molecular Zone (CMZ) using the 2D correlation function. To quantify the spatial anisotropy, we define the critical angle θ_{half} , as well as the anisotropy parameter $A \equiv \frac{\pi}{4\theta_{\text{half}}} - 1$. We find that the density structure is strongly anisotropic at the large scale (~ 100 pc), and the degree of spatial anisotropy decreases with the decreasing scale. At the scale of ~ 10 pc, the structure is still mildly anisotropic. In our analyses, we provide a quantitative description of the anisotropic density structure of gas in the CMZ, and the formalism can be applied to different regions to study their differences.

Key words: anisotropy — galactic centre — shear – correlation function

1 INTRODUCTION

Situated at the center of the Milky Way, the Central Molecular Zone (CMZ) is an unusually dense molecular cloud complex with a size of a few hundred parsecs (Launhardt et al. 2002). A total mass of $3 \times 10^7 M_{\odot}$ is found inside this region (Dahmen et al. 1998; Molinari et al. 2014). Observations indicate that the gas in the CMZ has high volume densities (with a mean value of $\sim 10^4 \text{ cm}^{-3}$, Li & Zhang 2020) and high column densities (about $\sim 10^{23} \text{ cm}^{-2}$, Lis & Carlstrom 1994).

In spite of the widespread presence of dense gas, the star formation efficiency (SFE) is about 10 – 100 times lower than the standard values (Kauffmann et al. 2013; Longmore et al. 2013a; Emsellem et al.

gravitational instability, turbulence, tidal force, cloud-cloud collision and shear etc. (Longmore et al. 2013a; Jeffreson et al. 2018; Kruijssen et al. 2019).

The shear on a cloud will cause a velocity difference between its near side and its far side to the Galactic center, which stretches the gas into long streams. The strength of shear can be quantified using the shear timescale, which is $t_{\text{shear}} = (\partial\Omega/\partial r \times r)^{-1}$. In the Milky way, shear is believed to be responsible for creating large-scale filamentary structures (Dobbs & Bonnell 2006). Some first hints on the importance of shear came from the discovery of kpc-sized filamentary structures (Li et al. 2013; Goodman et al. 2014; Wang et al. 2015). Further observations have found that the filamentary structures of sizes of a few to a few tens of pc tend to stay parallel to the Galactic disk (Li et al. 2016; Wang et al. 2015), indicating that shear is dynamically important on these scales. In some cases, shear can play a dominant role in determining the star formation activity: recent results from Li & Zhang (2020) indicate that shear alone is responsible for the observed low level of star formation seen in the CMZ region.

One way to reveal the role of shear is to study the alignment of filamentary structures (Li et al. 2016; Wang et al. 2015). However, this approach, although effective, is cumbersome to implement. Besides, the evolution of the interstellar medium is a multi-scale process, and ideally, we would like to know the role of shear over a range of scales. As studying the role of shear using the alignment of filamentary structures only allows us to probe the scales comparable to the lengths of the filaments, better methods are needed. In this paper, we develop a formalism to quantify the anisotropy of the density structure of the CMZ quantitatively using the 2D correlation function, with which the role of shear can be studied over a range of scales. In section 2, we present the data. In section 3, we describe the method and present the results. In section 4, we give a conclusion.

2 DATA

We use the 870 μm map from the APEX Telescope Large Area Survey of the Galaxy (ATLASGAL) (Schuller et al. 2009). The observations were carried out with the APEX 12 m submillimeter telescope in dust emission continuum with an angular resolution of $19.2''$ and a sensitivity of 50 Jy/beam. We assume that the CMZ region has a mean distance of 8.2 kpc, estimated from the updated distance to the Sgr A from Gravity Collaboration et al. (2019). The corresponding spatial resolution is ~ 0.76 pc. The size of the selected region is about $477 \text{ pc} \times 159 \text{ pc}$. The maps contain contaminations from the fore/background, and this amounts to around 10 % of the total flux (Li & Zhang 2020). Thus, the contributions from fore/background emission to the overall correlation should be insignificant.

3 METHODS AND RESULTS

3.1 The correlation function

Our data is taken from Schuller et al. (2009), from which the mass surface density can be calculated by using

$$N_{\text{H}_2} = \frac{F_\nu R_0}{B_\nu(T_{\text{D}})\Omega\kappa\mu m_{\text{H}}}, \quad (1)$$

where F_ν is the flux density, $R_0 \sim 100$ is the gas-to-dust ratio, Ω is the solid angle of the telescope

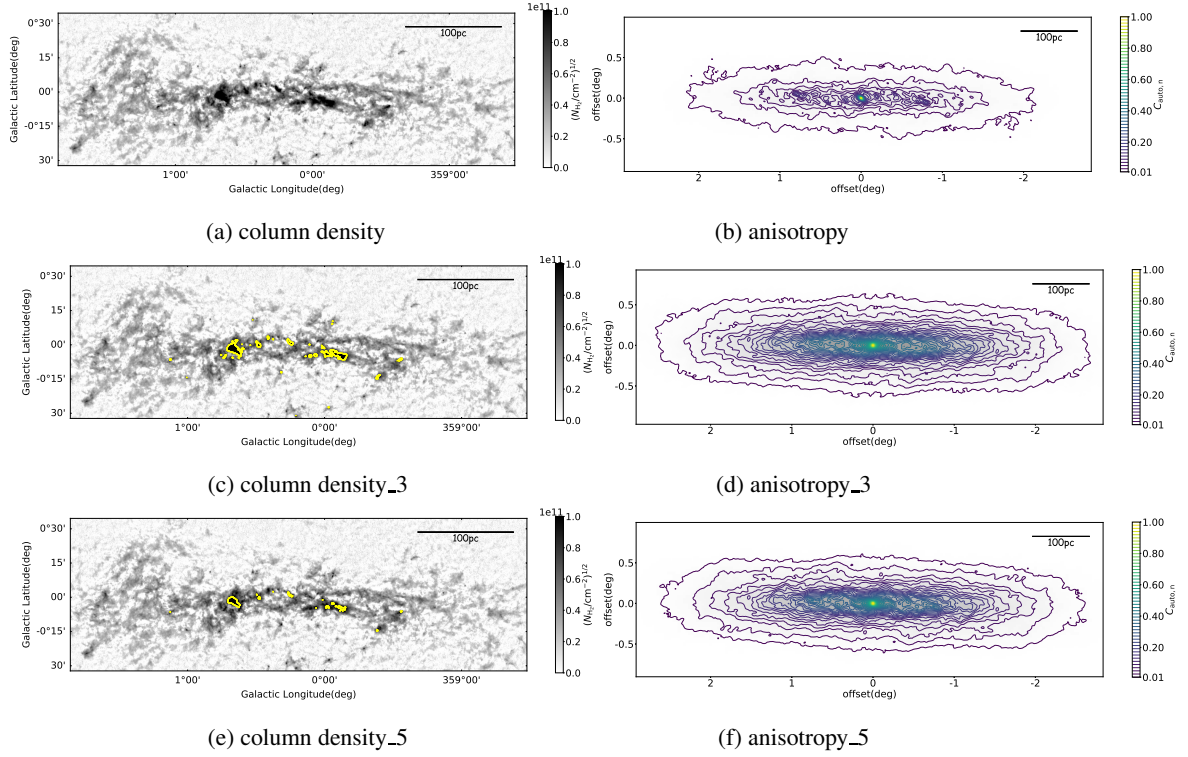


Fig. 1: Left panels: Column density distribution in the Central Molecular Zone of the Galactic center observed by the survey:the APEX Telescope Large Area Survey of the Galaxy (ATLASGAL) at $870 \mu\text{m}$, with a beam size of $19.2''$ and a typical noise level of $50\text{-}70 \text{ mJy/beam}$. The horizontal size bar in upper right corner indicates a length of 100 pc . The yellow contours in Figure 1c show the region where the flux intensity is more than 3 Jy/beam ($8.31 \times 10^{21} \text{ cm}^{-2}$). The yellow contours in Figure 1e shows the region where the flux intensity is more than 5 Jy/beam ($1.385 \times 10^{22} \text{ cm}^{-2}$). **Right panels:** 2D correlation functions $C_{\text{auto},n}$. In Figure 1b, the correlation function is computed using the emission map. In Figures 1d and Figure 1f, we plot the correlation function computed from clipped emission maps where we set the value of regions where $I > 3, 5 \text{ Jy/beam}$ to $I_{\text{max}} = 3, 5 \text{ Jy/beam}$, which correspond to $N_{\text{H}_2} = 8.31 \times 10^{21} \text{ cm}^{-2}$ and $1.385 \times 10^{22} \text{ cm}^{-2}$.

molecules, (Kauffmann et al. 2008), and m_H is the mass of an hydrogen atom. We adopt a uniform temperature of $T_D = 20 \text{ K}$ (Ginsburg et al. 2016; Molinari et al. 2010; Traficante et al. 2011). At $870 \mu\text{m}$, $\kappa = 1.85 \text{ cm}^2 \text{ g}^{-1}$ (Ossenkopf & Henning 1994) and

$$B_\nu(T_D) = \frac{2h\nu^3}{c^2} \frac{1}{e^{\frac{h\nu}{kT}} - 1}. \quad (2)$$

Here, we have assumed a uniform temperature for the whole region. In reality, the temperature varies by around 5 K , leading to an uncertainty of about 20% for individual regions. As the errors of surface density caused by temperature variations are small compared to the intensity variations, the contribution from temperature to the overall correlation should be minimal.

To quantify the anisotropy of the density structure, we evaluate C_{auto} , which is the 2D correlation

is

$$f(k_1, k_2) = \int_{-\infty}^{\infty} \int_{-\infty}^{\infty} f(x, y) e^{-i(k_1 x + k_2 y)} dx dy. \quad (3)$$

We first calculated the power spectrum in the k -space. f^\dagger is the conjugation of f .

$$P(k_1, k_2) = f(k_1, k_2) f^\dagger(k_1, k_2). \quad (4)$$

Then the correlation function in the real space, C_{auto} is obtained by the inverse transform

$$C_{\text{auto}}(x, y) = \frac{1}{4\pi^2} \int_a^b \int_a^b P(k_1, k_2) e^{i(k_1 x + k_2 y)} dk_1 dk_2. \quad (5)$$

The column density map of the CMZ is shown in Figure 1a. The normalized 2-D correlation function ($C_{\text{auto},n} \equiv C_{\text{auto}}/C_{\text{auto},\text{max}}$) based on the flux data is shown in Figure 1b. Note that calculations done in the Fourier space assumes a periodic boundary condition. To minimize boundary effects, we add zero paddings around our maps before performing the calculations. We note that in some cases, a very significant amount of emission is contained in a very small region (e.g. the Sgr B2 region). To evaluate their contributions to the overall correlation, we experiment with performing clipping operations to the data at regions where the flux is larger than a certain threshold of 3 Jy/beam ($8.31 \times 10^{21} \text{ cm}^{-2}$) and 5 Jy/beam ($1.385 \times 10^{22} \text{ cm}^{-2}$), separately. This is achieved by setting the values of regions where the flux is above a threshold to that threshold. We set flux data more than 3, 5 Jy/beam ($8.31 \times 10^{21} \text{ cm}^{-2}$, $1.385 \times 10^{22} \text{ cm}^{-2}$) to $I_{\text{max}} = 3, 5$ Jy/beam ($8.31 \times 10^{21} \text{ cm}^{-2}$, $1.385 \times 10^{22} \text{ cm}^{-2}$). The regions where the flux data more than 3, 5 Jy/beam ($8.31 \times 10^{21} \text{ cm}^{-2}$, $1.385 \times 10^{22} \text{ cm}^{-2}$) are marked yellow in Figure 1c and Figure 1e, separately. The clipping operation effectively reduces the dynamic range of the maps. The correlation functions computed from these clipped maps are presented in Figure 1d and Figure 1f. By comparing the clipped results (Figure 1d and Figure 1f) to the unclipped ones (Figure 1b), we are able to evaluate the contribution to the correlation function from regions of different surface densities.

From all these correlation functions, we observe that the contours in the centre (at small scales) are nearly roundish, but at larger scales, the contours are elliptical where the long axes of the ellipses are aligned with the mid-plane of the Milky Way. This is an indication that shear is dynamically important in the region.

3.2 Quantifying the spatial anisotropy

To further quantify the spatial anisotropy measured as a function of the scale, we divide the region into rings of different radii. Each ring is characterized by the l parameter, which is the distance from the origin (Figure 2a). For each ring, we plot the value of the correlation function against θ , which is the angle measured with respect to the Galactic mid-plane. We have considered all the points. And θ has been transformed to the range $(0, \frac{\pi}{2})$ (Figure 2b). Due to symmetry, the θ is between 0 and π . Additional, we assume that the structure of the CMZ is symmetric had we turned it upside down (horizontal mirror symmetry). Thus, we only need to plot θ between 0 and $\frac{\pi}{2}$.

As an example, we plot the results from a ring at $l \sim 33.4 - 35.8$ pc. The ring width Δl is 10 pixels, about 2.4 pc. In Figure 3a, we plot the $C_{\text{auto},n}$ against θ . Here, the spatial anisotropy can be seen from the

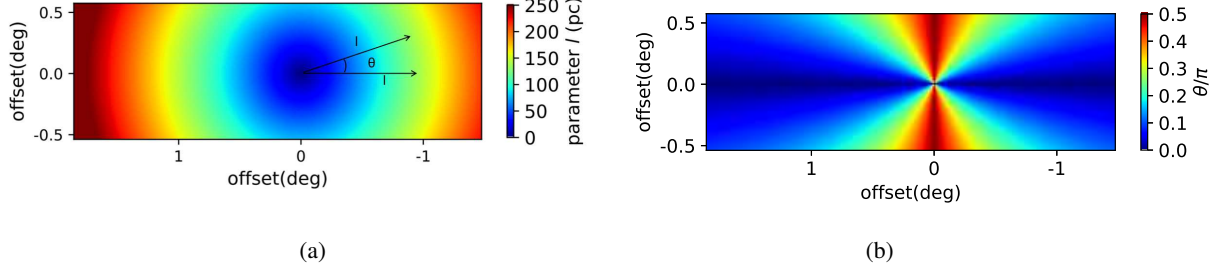


Fig. 2: (a) The region is divided with different radii and l is the distance from the origin. (b) The region is divided with different angles, we symmetrize it into the range of 0 to $\frac{\pi}{2}$, the colorbar is θ/π .

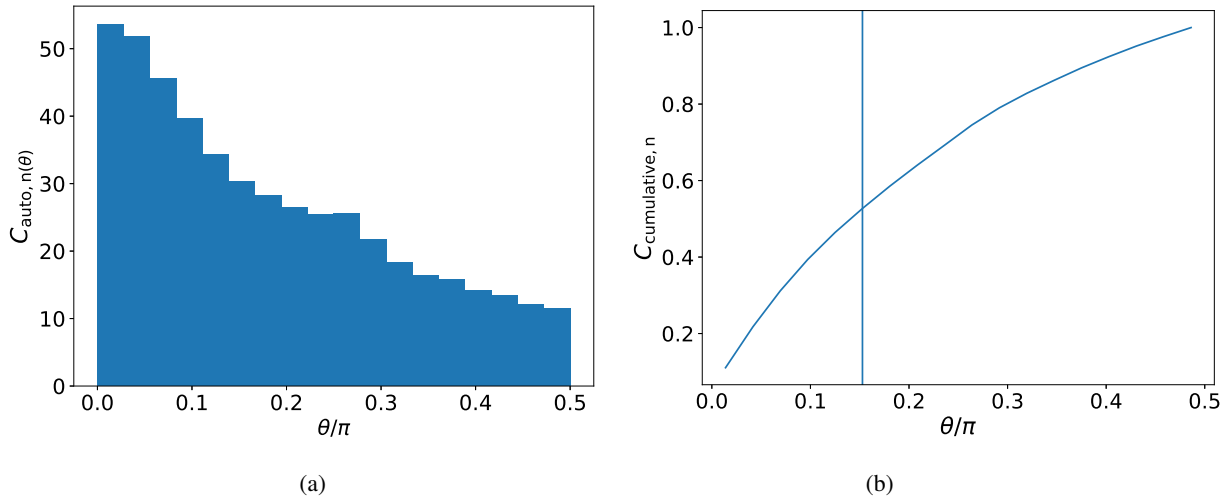


Fig. 3: (a) The distribution of $C_{\text{auto},n}$ against θ . (b) $C_{\text{cumulative},n}$ - θ/π relation. $C_{\text{cumulative},n}$ is the normalized cumulative correlation function. The vertical line shows where the $C_{\text{cumulative},n}$ is 0.5.

To quantify the spatial anisotropy at scale l , we define the so-called half correlation angle θ_{half} , which is the critical angle within which half of the correlation function is contained. To derive θ_{half} , we define the so-called cumulative correlation function $C_{\text{cumulative}}(\theta) = \int C_{\text{auto},n}(\theta)d\theta$, then we normalize it, obtaining the normalized cumulative correlation function $C_{\text{cumulative},n}(\theta) = C_{\text{cumulative}}(\theta)/C_{\text{cumulative,max}}(\theta)$. The θ_{half} is obtained by solving $C_{\text{cumulative},n}(\theta) = 0.5$. The procedure is illustrated in Figure 3b. For isotropic structures, $\theta_{\text{half}} = \frac{\pi}{4}$, whereas for structures that are preferentially aligned with the disk mid-plane, $\theta_{\text{half}} < \frac{\pi}{4}$. An example of how we derive θ_{half} is presented in Figure 3b.

The above-mentioned exercise allow us to study how the spatial anisotropy evolve as the function of the scale. In Figure 4a, we plot θ_{half} against the scale, and where θ_{half} decreases with the increasing scale. This indicates that the spatial anisotropy is stronger at larger scales.

We further define the the anisotropy parameter

$$A \equiv \frac{\pi}{4 \theta_{\text{half}}} - 1. \quad (6)$$

$A > 0$ means that at the scale of interest, the density structure is anisotropic, and the value of A measures the degree of anisotropy. For an homogeneous region, the correlation strength is evenly distributed between 0 and $\frac{\pi}{2}$. $\theta_{\text{half}} = \frac{\pi}{4}$, A will be 0. As $\theta = 0$ corresponds to the direction along which the correlation

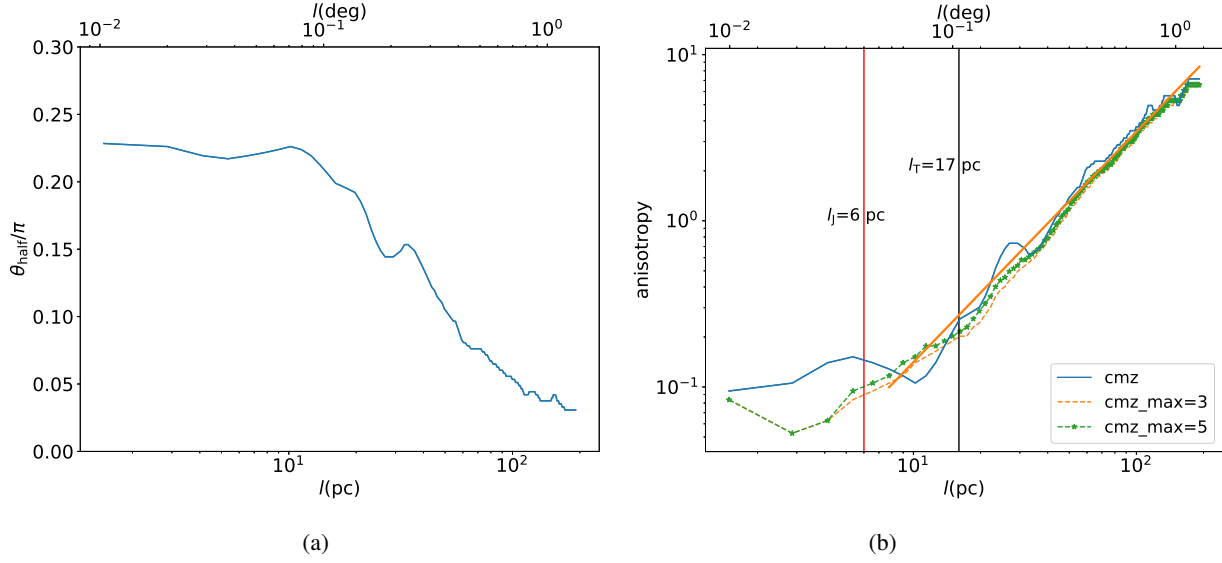


Fig. 4: (a) $\theta_{\text{half}}/\pi - l$ relation. θ_{half} decreases with l in the CMZ. (b) Anisotropy- l relation. The left vertical line indicates where the Jeans lengths l_J (6 pc) and the right vertical line represents the Toomre lengths l_T (17 pc) estimated by Henshaw et al. (2016). The solid line is the anisotropy- l distribution calculated with raw data. The dashed line is the anisotropy- l distribution calculated by setting raw data more than 3 Jy/beam ($8.31 \times 10^{21} \text{ cm}^{-2}$) to $I_{\text{max}} = 3 \text{ Jy/beam}$ ($8.31 \times 10^{21} \text{ cm}^{-2}$). The dashed line with stars is the anisotropy- l distribution calculated by setting raw data more than 5 Jy/beam ($1.385 \times 10^{22} \text{ cm}^{-2}$) to $I_{\text{max}} = 5 \text{ Jy/beam}$ ($1.385 \times 10^{22} \text{ cm}^{-2}$). The straight line at scales larger than 10 pc is the linear fit of data, $\log_{10} A \approx 1.4 \log_{10} l - 2.2$.

also plot regions where we have chosen different I_{max} . We note that at scales below 10 pc, the anisotropy parameter depends on the value of I_{max} . Thus, we should only interpret results from scales larger than 10 pc, as only in this range do results from different I_{max} converge. At scales larger than 10 pc, we perform a fit to our data and find $\log_{10} A \approx 1.4 \log_{10} l - 2.2$. The anisotropy is strong on the large scale, and it decreases with decreasing scale. At around $l = 10 \text{ pc}$, the density structure is still moderately anisotropic.

We further add the two vertical lines indicating the Toomre length $l_T \approx 17 \text{ pc}$ and the Jeans length $l_J \approx 6 \text{ pc}$ (Henshaw et al. 2016), respectively. The Jeans length is the length scale above which the gravity can induce collapse, and the Toomre length is the length below which self-gravity is stronger than shear. The density structure is expected to be anisotropic at $l > l_T$, and this is confirmed by our results. Apart from this, we can still observe a significant amount of anisotropy at $l_T > l > l_J$.

4 CONCLUSIONS

We study the density structure of gas in the Central Molecular Zone by applying the 2D correlation function. We find that the density structure is strongly anisotropic where the correlation is strong along the l direction, suggesting that shear is dynamically important.

To quantify anisotropic density structure, we define the half-correlation angle θ_{half} and the anisotropy

anisotropic at $l = 10$ pc. The between 10 pc and 100 pc, we find that

$$\log_{10} A \approx 1.4 \log_{10} l - 2.2 .$$

We propose a picture where at the large scale ($l > 10$ pc), shear is dynamically important such that it can change the density structure of the gas significantly, and its strength diminishes as one moves to smaller scales. At ($l \lesssim 10$ pc), as shear should have the roughly same strength as the self-gravity, thus the gas can enter a state called “shear-enabled pressure equilibrium” (Li & Zhang 2020). The formalism developed here can be used to study the role of shear in different regions in a quantitative fashion and reveal the differences.

Acknowledgements We thank the anonymous referee for a constructive review report that improved this paper. Lei Qian is supported by NSFC No. U1631237 and the Youth Innovation Promotion Association of CAS (id. 2018075). Guang-Xing Li is supported by a starting grant from Yunnan University, and NSFC grant W820301904. The paper makes use of data from the ATLASGAL survey carried out by the APEX telescope.

References

- Dahmen, G., Huttemeister, S., Wilson, T. L., et al. 1998, *A&A*, 331, 959
- Dobbs, C. L. & Bonnell, I. A. 2006, *MNRAS*, 367, 873. doi:10.1111/j.1365-2966.2006.10146.x
- Emsellem, E., Renaud, F., Bournaud, F., et al. 2015, *MNRAS*, 446, 2468. doi:10.1093/mnras/stu2209
- Gravity Collaboration, Abuter, R., Amorim, A., et al. 2019, *A&A*, 625, L10. doi:10.1051/0004-6361/201935656
- Goodman, A. A., Alves, J., Beaumont, C. N., et al. 2014, *ApJ*, 797, 53. doi:10.1088/0004-637X/797/1/53
- Ginsburg, A., Henkel, C., Ao, Y., et al. 2016, *A&A*, 586, A50. doi:10.1051/0004-6361/201526100
- Henshaw, J. D., Longmore, S. N., & Kruijssen, J. M. D. 2016, *MNRAS*, 463, L122. doi:10.1093/mnrasl/slw168
- Jeffreson, S. M. R., Kruijssen, J. M. D., Krumholz, M. R., et al. 2018, *MNRAS*, 478, 3380. doi:10.1093/mnras/sty1154
- Kauffmann, J., Bertoldi, F., Bourke, T. L., et al. 2008, *A&A*, 487, 993. doi:10.1051/0004-6361:200809481
- Kauffmann, J., Pillai, T., & Zhang, Q. 2013, *ApJ*, 765, L35. doi:10.1088/2041-8205/765/2/L35
- Kruijssen, J. M. D., Dale, J. E., Longmore, S. N., et al. 2019, *MNRAS*, 484, 5734. doi:10.1093/mnras/stz381
- Lis, D. C. & Carlstrom, J. E. 1994, *ApJ*, 424, 189. doi:10.1086/173882
- Launhardt, R., Zylka, R., & Mezger, P. G. 2002, *A&A*, 384, 112. doi:10.1051/0004-6361:20020017
- Longmore, S. N., Bally, J., Testi, L., et al. 2013, *MNRAS*, 429, 987. doi:10.1093/mnras/sts376
- Li, G.-X., Wyrowski, F., Menten, K., et al. 2013, *A&A*, 559, A34. doi:10.1051/0004-6361/201322411
- Li, G.-X., Urquhart, J. S., Leurini, S., et al. 2016, *A&A*, 591, A5. doi:10.1051/0004-6361/201527468
- Li, G.-X. & Zhang, C.-P. 2020, *ApJ*, 897, 89. doi:10.3847/1538-4357/ab8c47
- Molinari, S., Swinyard, B., Bally, J., et al. 2010, *A&A*, 518, L100. doi:10.1051/0004-6361/201014659
- Molinari, S., Bally, J., Glover, S., et al. 2014, *Protostars and Planets VI*, 125. doi:10.2458/azu_uapress9780816531240-ch006

Schuller, F., Menten, K. M., Contreras, Y., et al. 2009, *A&A*, 504, 415. doi:10.1051/0004-6361/200811568

Traficante, A., Calzoletti, L., Veneziani, M., et al. 2011, *MNRAS*, 416, 2932. doi:10.1111/j.1365-2966.2011.19244.x

Wang, K., Testi, L., Ginsburg, A., et al. 2015, *MNRAS*, 450, 4043. doi:10.1093/mnras/stv735

Wang, K., Testi, L., Burkert, A., et al. 2016, *ApJS*, 226, 9. doi:10.3847/0067-0049/226/1/9